Coherent population transfer among Rydberg states by subpicosecond, half-cycle pulses

N. E. Tielking and R. R. Jones
Department of Physics, University of Virginia, Charlottesville, Virginia 22901
(Received 13 February 1995)

Ultrashort, unipolar electric-field pulses have been used to coherently redistribute population between Rydberg states in sodium. The population in several Rydberg states is recorded simultaneously as a function of peak field. In addition, two temporally separated pulses have been used to interferometrically characterize the redistribution process. In the lowest fields, the experimental results are in agreement with the predictions of lowest-order perturbation theory. At slightly higher fields, still well below the ionization threshold, the redistribution process becomes nonperturbative, and a numerical integration of the time-dependent Schrödinger equation must be used to achieve partial agreement between theory and experiment.

PACS number(s): 32.80.Rm

I. INTRODUCTION

Recently, subpicosecond, nearly unipolar electromagnetic field pulses have been used to study nonperturbative Rydberg-atom–pulsed-field interactions [1,2]. These pulses have been referred to as "half-cycle" pulses (HCPs) because the time dependence of the electric field resembles that of one-half of an optical cycle of terahertz band radiation [3]. The extremely short duration of these pulses makes it possible to study Rydberg atoms over time periods that are short compared to the characteristic time scales of the atomic system (i.e., the classical Kepler period of the Rydberg electron). In addition, the unipolar nature of HCPs makes the dynamic response of atoms to these pulses significantly different from that in short, multicycle pulses [1,2].

The goal of previous experiments has been to characterize the ionization of Rydberg atoms by HCPs [1,2]. The results of those experiments are most easily understood using classical mechanics. The large density of essential states coupled with the broad coherent bandwidth in the pulse makes quantum calculations virtually impossible. Although such calculations have been performed on scaled down systems [4,5], the physical insight gained from the classical treatment is far greater than any derived from the large scale quantum calculations. In any case, both quantum and classical mechanics describe the ionization process as a complicated dynamic evolution through many bound intermediate states into a broad spectrum of continuum energies and angular momenta. The goal of the experiments described here is to characterize the redistribution process that precedes ionization.

We have observed population transfer from a single Rydberg state to many others during a HCP. We have studied the evolution of the redistribution process as a function of the peak HCP field and the principal and angular momentum quantum numbers of the initial state. In addition, we have probed the coherence of the final-state population using a bound-state interferometric technique [6] that utilizes two temporally separated HCPs. The interferometric method is used as a spectroscopic tool to identify which single and multiphoton transitions contribute to the redistribution process.

By reducing the field amplitude in the HCP to well below that required for ionization, the number of interacting states can be kept at a level that is feasible for quantum calculations. In general, the results of these calculations are in qualitative agreement with the experimental results. In the following sections we describe the experimental and theoretical techniques and results. We conclude with several remarks regarding implications for future experiments.

II. EXPERIMENTAL METHOD

The experimental apparatus is nearly identical to those described previously [1,2,7]. Two tunable, 10-nsec dye laser pulses are used to excite a thermal beam of ground-state Na atoms through the $3p_{1/2}$ level to a n^*s or n^*d, $|m_j|=\frac{1}{2}$, Rydberg state. Here n^* refers to the integer that is nearest to the effective quantum number, $\mu=n-\delta$, where n is the principal quantum number and δ is the angular-momentum-dependent quantum defect. A particular n^*l Rydberg state is selected by changing the frequency of the second dye laser. A diagram of the Rydberg spectrum is shown in Fig. 1.

The HCP is generated by illuminating a biased, GaAs wafer (2 cm×2 cm×0.5 mm) with a 120-fsec, 780-nm laser pulse from an amplified, self-mode-locked Ti:sapphire oscillator [3]. The far-infrared (FIR) radiation transmitted through the wafer is collected with a parabolic mirror and directed toward the Rydberg atoms. The peak electric field in the pulse varies linearly with the bias voltage across the GaAs and can be changed continuously from 0 to > 50 kV/cm [3]. The frequency spectrum and temporal shape of the HCP are inferred from electric-field autocorrelations and optical gating techniques [3]. The pulse shapes shown in Fig. 2 are derived from two-pulse ionization of a Rydberg state and are consistent with previous measurements using the techniques described previously [3]. Figure 2(a) shows the temporal

 ©1995 The American Physical Society

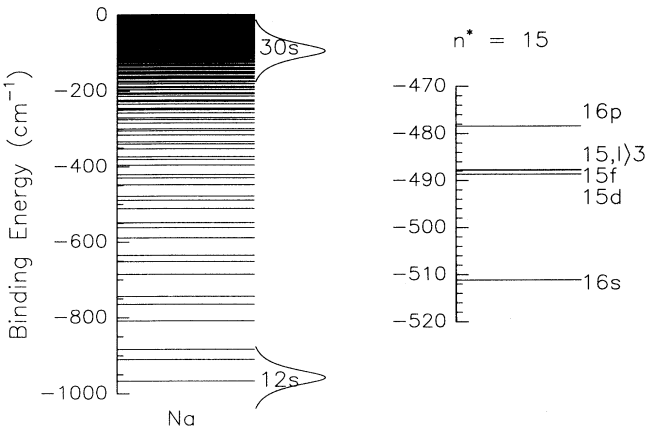

FIG. 1. Energy-level diagram of the bound states in Na for states with principal quantum number $n > 10$. The bell-shaped curves to the right of the main diagram show the approximate frequency spectrum of the HCP that is used to redistribute the population. Note that for low-n values single-photon transitions between low angular momentum states are only possible in the extreme wings of the pulse spectrum, but many levels are coupled by the peak frequencies in the spectrum for high-n-states. An enlarged section of the $n^* = 15$ manifold of states is also displayed to show the relative positions of the different angular momentum states for each principal quantum number.

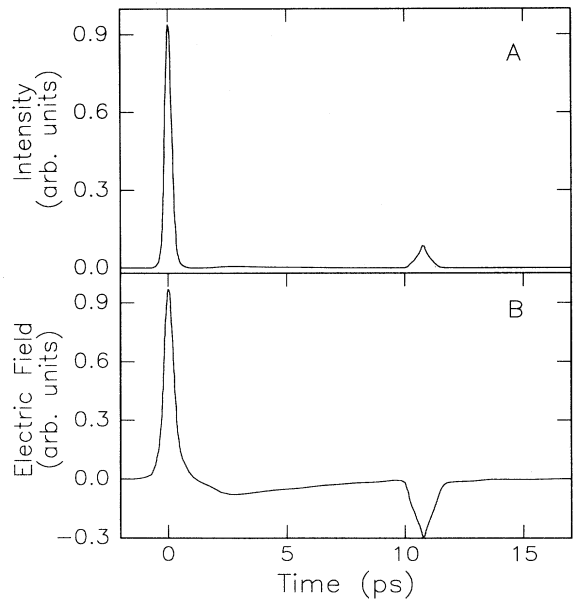

FIG. 2. Plots of the (A) intensity and (B) electric field in the HCP inferred from measurements of ionization of Rydberg states with two time-delayed pulses. The error in the field amplitude is approximately 10% of the *peak* field. Note that the intensity distribution in (A) is predominantly that of a unipolar pulse, with a small secondary peak displaced by 11 ps from the main feature. (B) clearly shows that the sign of the "reflection" peak and the low amplitude "negative tail" have the opposite polarity of the main peak.

intensity profile. Note that essentially 90% of the pulse energy comes in a unipolar pulse of approximately 0.5 psec duration. A second "reflection" pulse, created by imperfect transmission of the HCP through the GaAs wafer, appears 11 ps after the initial pulse. The time dependence of the *electric field* is shown in Fig. 2(b). Note that the "reflection" pulse has a polarity that is opposite that of the main pulse. In addition, a "negative tail," which follows immediately after the main pulse and extends at least tens of picoseconds, is clearly visible. Since the charge state of the GaAs wafer is identical at the beginning of each laser pulse, the time-integrated electric field in the HCP must be zero. However, as Fig. 2(b) clearly shows, the amplitude of the negative tail is much smaller than that of the main pulse, and its duration is much longer. The recharging of the GaAs wafer takes place over microsecond time scales. Therefore, after the first few picoseconds, the field amplitude in the negative tail can be orders of magnitude smaller than the main pulse and still satisfy the condition of zero time-integrated field. Previous measurements have shown that the ionization probability due to the full pulse, including the "reflection" and "negative tail," is significantly different from the ionization probability due to the main half-cycle component alone [7]. The effect of the HCP temporal structure on the redistribution process will be discussed in forthcoming sections.

As shown in Fig. 3, the HCP crosses the dye laser and atomic beams at right angles. Before reaching the interaction region, the HCP propagates through a second GaAs wafer that can be used as an optical gate. The transmission of the HCP through this "attenuating" wafer can be dramatically reduced on a 100-fs time scale by illuminating the wafer with a second 120-fs laser pulse [3,7]. The absorption of the laser pulse on the surface of the GaAs promotes electrons to the conduction band, transforming the wafer surface into a transient conductor. During the 120-fs laser pulse, the transmission of the FIR energy through the wafer is reduced by approxi-

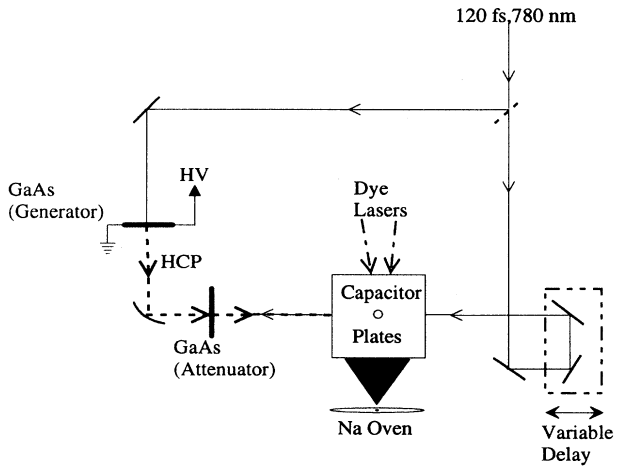

FIG. 3. Schematic of the experimental apparatus showing the interaction region, Na oven, dye lasers, HCP generator, and the transient attenuator.

mately a factor of 10. This reduced transmission persists over a nanosecond time scale. Therefore, by exciting the "attenuating" wafer at the appropriate time, the amplitude of the nonunipolar components of the pulse can be significantly attenuated with respect to the main HCP. Since the presence of the nonunipolar features alters the ionization probability, the appropriate delay between the laser pulses used to produce the HCP and gate can be obtained by observing the ionization signal as a function of delay between the two pulses [7].

The Rydberg atoms interact with the HCP between two parallel capacitor plates that are separated by 1.5 cm. The distribution of final Rydberg states is measured using state-selective field ionization. After the HCP, a 5-μs high-voltage ramp (peak voltage <10 kV) ionizes any Rydberg states in the interaction region. Each Rydberg state ionizes when the electric field in the interaction region reaches a critical value, which depends on the zero-field binding energy of the state. The electrons that are produced are pushed through a 1-mm-diam hole in the upper capacitor plate and are collected by a microchannel plate detector. Electrons originating in different Rydberg levels are ionized at different times during the ramp, and therefore reach the detector at different times. Hence, the electron time-of-flight (TOF) spectrum yields the final Rydberg-state distribution.

Figure 4(a) shows a typical TOF spectrum when a single Rydberg state is populated, and Fig. 4(b) shows the distribution of final states created by a HCP. Note that several new peaks have appeared in the TOF spectrum in Fig. 4(b) compared to that in Fig. 4(a). Although it is trivial to resolve states with the same angular momentum and different principal quantum numbers, the resolution between angular-momentum states with a common principal quantum number is less than perfect. Although the resolution is typically much better than that shown in Fig. 4(b), the effect of imperfect resolution on our results is non-negligible and will be discussed in detail later in the paper. The narrow, closely spaced peaks on the left in Fig. 4(b) are due predominantly to population in the lowest three angular-momentum states $l=0$, 1, and 2. The broad peak at later times in Fig. 4(b) is due to population in the higher-angular-momentum states. During the several microsecond high-voltage ramp, the orbital angular-momentum vector of these states precesses in the earth's magnetic field. Due to this precession, the projection of the orbital angular momentum on the electric-field axis, m, is not constant and can be much greater than 2. These high-m states ionize at a field that is approximately a factor of 2 higher than that for the low-m levels. Therefore, the earth's magnetic field allows us to easily separate final states with $l,m>2$ from those with $l,m\leq 2$.

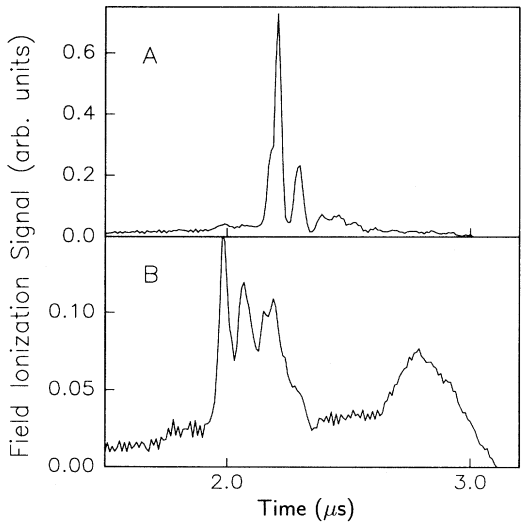

FIG. 4. Time-of-flight (TOF) electron spectrum generated by field ionization of (A) the 18d state, and (B) the redistributed population from the 18d state after its interaction with a HCP. The double peak structure in (A) is due to the dynamics of the field ionization process that causes the 18d state to ionize predominantly along two different adiabatic paths. In (B) the narrow peaks (from left to right) are due to the population in the 18$^*p$, 18 $l>2$, 18$^*s$, and 18d states with $m<3$. The broad peak at later times is due to the population in the $l,m>2$ levels. The high-l,m states ionize hydrogenically at a field approximately twice that of the low-l,m states. The high-m states are populated through the precession of the electron's angular momentum in the earth's magnetic field.

The peak field in the HCP is determined by measuring the ionization probability for a given state as a function of the HCP field. Recent ionization experiments utilizing the transient attenuator described above have shown that the measured ionization probabilities agree with those predicted by classical and quantum calculations to within the accuracy of our pulse energy detector [7]. Therefore, daily comparisons of new ionization data with previously calibrated data yield accurate and consistent peak field values.

It is important that we mention some limitations of the state-selective ionization technique used in the experiments. The resolution and accuracy of our measurements depend on the slew rate of the high-voltage ramp and on the width of the time bins used to collect the signal for a single Rydberg state. The lower the slew rate, the greater the resolution between individual ionizing states. However, the slew rate is determined by the duration of the field ramp, which is limited to a few microseconds due to the transit time of the atoms beneath the extraction hole. Therefore, we are unable to resolve each angular-momentum state in the TOF spectrum. If many angular-momentum states are populated, it is necessary to reduce the width of each time bin in order to prevent contamination from the signal due to population in other states. Unfortunately, reducing the bin width can cause some population in the state of interest to go undetected, making relative state amplitude assignments difficult.

Typically, the maximum voltage in the ramp is adjusted to be only slightly larger than necessary to ionize the states of interest. As the voltage ramp rolls over near the peak voltage, the slew rate is drastically reduced. Therefore, significantly higher resolution can be obtained without substantially increasing the delay between excitation and detection of the Rydberg states. Unfortunately, since for a given value of n^* the $l,m>2$ states ionize at a

field that is nearly a factor of 2 higher than that needed to ionize the low-m levels, ionization of the low-m states must take place in the center of the ramp and not near the maximum if the $l,m>2$ states are to be detected. Therefore, detection of the high-l,m states necessarily implies decreased selectivity in the detection of the lower-l states.

III. SINGLE-PULSE REDISTRIBUTION

Two different experiments are used to study the redistribution process. In the first experiment, the population in several Rydberg states is measured as a function of the peak field in a single HCP. Measurements are made with the transient "attenuator" in two different configurations: (i) allowing the entire pulse to enter the interaction region, and (ii) gating the pulse so that the Rydberg atoms see only the main half-cycle component. The results reported here are for population transfer from n^*s or n^*d states to all allowed states n^*l.

The final-state distribution from an initial 18^*d state is plotted in Fig. 5 as a function of peak field in an unattenuated HCP. Figure 5 also shows the population distribution from the same initial state, using a "clean" pulse with the negative tail and reflection pulse significantly attenuated. Aside from small differences near the peak in the p-state amplitude, the curves produced with a "clean" pulse are essentially identical to those produced with the full pulse. This observation holds for a transfer out of initially populated s states as well. In general, the nonunipolar components of the pulse (hereafter referred to as the "tail" of the pulse) do not significantly affect the redistribution process at these low fields. However, as discussed previously, the pulse tail does contribute to ionization, which becomes non-negligible for fields >7 kV/cm for the initial $18d$ state of Fig. 5.

Apparently, the effects of the pulse tail become significant at intermediate fields lower than those needed for ionization, but greater than that required for substantial redistribution. This observation can be understood in terms of saturation of the transition amplitudes to the different final states. Figure 5 shows that the population transferred to the p state increases rapidly, saturates at a level $>30\%$, and then decreases as the electric field is monotonically increased. Lowest-order perturbation theory predicts an increase in the p-state population, which is proportional to the incident intensity. As Fig. 2(a) shows, the intensity during the main pulse is approximately ten times higher than the peak intensity in the tail. Therefore, as long as the p-state population is well below saturation, the effects of the tail will be small compared to those of the main HCP. However, once the p-state population has saturated and actually decreases with increasing field strength, the net population transfer to the p state during the pulse tail can actually be greater than that in the main pulse. Hence, one expects the effects of the tail to be much more important in fields where one or more transitions are being driven past saturation (i.e., a Rabi phase of $>\pi$). In fact, small differences in the final-state populations begin to appear at fields comparable to those required to saturate the p-state amplitude.

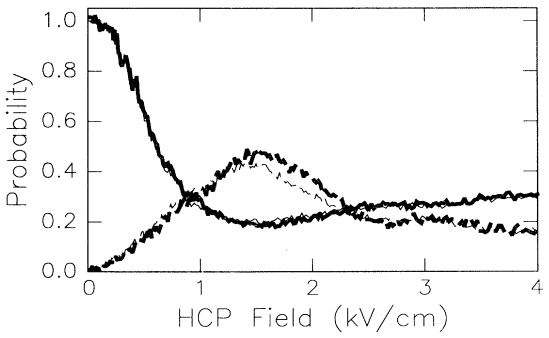

FIG. 5. Population in the 18^*d (solid curve) and 18^*p (dashed curve) states a function of the HCP field. The initial state is 18^*d. The bold curve shows the redistribution caused by a "clean" pulse with the "negative tail" and reflection pulse significantly attenuated. The light curve shows the redistribution from the full unattenuated pulse. Note that there is little quantitative difference in the curves for field values less than or comparable to that which maximizes the p-state population.

In the forthcoming sections, we will only consider field strengths that are within a factor of 2 or so of the p-state saturation field. Therefore, even though most of the measurements are made with a clean pulse, the tail of the pulse is not important in this low-field regime and it is not necessary to attenuate it. We will no longer distinguish between data taken with "clean" and "unclean" pulses.

The traces shown in Fig. 5 were obtained using a voltage ramp whose amplitude was slightly larger than necessary for ionization of the $18d$ state. Therefore, no information regarding the high-l,m states was obtained. In addition, relatively wide time bins were used to ensure that all of the d- and p-state signals were collected. As a consequence the curves contain some contributions from other states, particularly at the high end of the field scale, where many other states are excited.

In the next few paragraphs, we discuss and compare the qualitative aspects of the d-state and s-state redistribution processes. The final-state population from an initial 19^*d state is shown in Fig. 6(a), while that from the 19^*s level is displayed in Fig. 7(a). The qualitative aspects of these distributions are representative of similar plots for all of the s and d states studied, $15<n^*<25$. The strong qualitative differences between the s- and d-state redistributions are evident. The responsibility for these differences rests mainly on the nonzero quantum defects of the s, p, and d states in Na.

First, consider the d-state redistribution of Fig. 6(a). The d state rapidly depletes due to its interaction with high-l and -p states. A clear minimum in the d-state population occurs very near to the field value that maximizes the p-state signal. The high-l curve rises rapidly due to f-state population, saturates, and then slowly decreases. In low fields, the d state is coupled to only p and f states in the dipole approximation. In addition, the fact that the bandwidth of a true HCP is peaked at zero frequency, combined with the substantial decreases in the cross sec-

tion for n^* changing transitions restricts low-field transitions to the nearest f and p states only. In Na, the cross sections for $\Delta n^*=0$ transitions between d and f or d and p states are nearly identical. For the range of n states studied, the d to f transitions occur at a frequency of <1 cm^{-1} and the d to p transition frequencies are <9 cm^{-1}. Therefore, the ≈ 30 cm^{-1} bandwidth of the HCP, which is peaked near zero, causes the transition rate from d to p to be slightly lower than that from d to f. Indeed we observe that population in the high-l states (including the f level) grows faster than the p-state population.

At higher fields, the initial d state is depleted and population in the f and p states can be transferred back to the initial d state, or to other levels. The p state is only coupled to s and d states in the dipole approximation. However, because the s-to-p transition frequency is approximately three times higher than the p to d frequency, the dominant p-state transition is back to the d state. On the other hand, the f-state couplings to the d and g states are essentially the same due to the nearly identical cross sections and <1-cm^{-1} transition frequencies. Hence, the f-to-g coupling acts as a "leak" for population out of the p-d-f, three-level system into the higher-l states. Lower probability transitions at higher frequencies to states with different n^*, as well as multiphoton couplings to these other levels prevent the high-l states from trapping all of the initial-state population. Ionization is negligible for HCP fields <6 kV/cm for the $n^*=19$ levels.

The redistribution process is dramatically different for initially populated s states. The s levels are only coupled to p states. However, as discussed above, the s-to-p transition rate is significantly smaller than the p-to-d rate due to the larger s-to-p transition frequency, particularly for the lower n^* states. Therefore, compared to the d state, the depopulation of the s state occurs much more slowly with increasing field strength. In addition, the rapid p-to-d transition rate limits the maximum p-state population. Furthermore, population of the f and higher-l states can only be achieved by the sequential or simultaneous absorption of at least three photons. Hence, much higher fields are necessary to saturate the population in the high-l states.

The curves in Figs. 6 and 7 are the result of several different HCP field scans using different time bin widths and peak ramp voltages. In both of the figures, the high-l

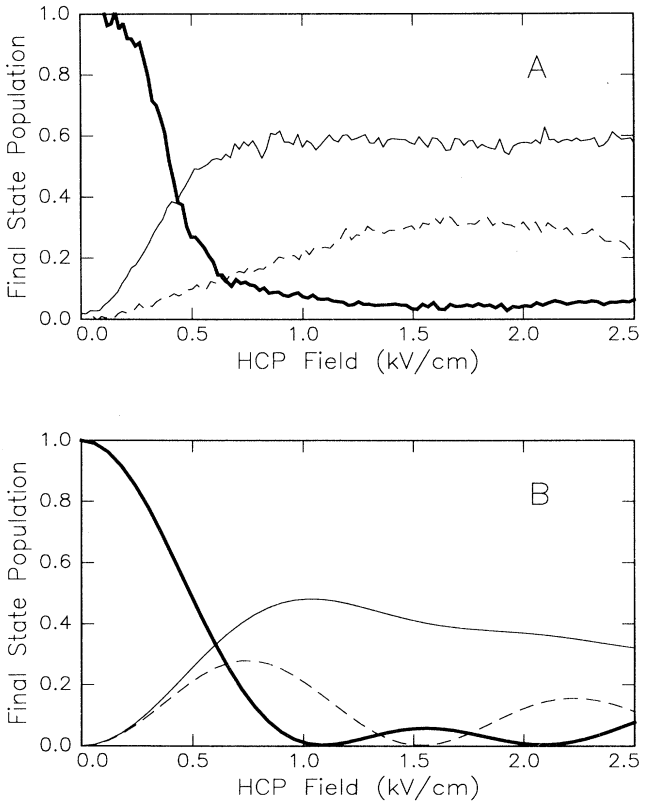

FIG. 6. Population in different $n^*=19$ states as a function of the HCP field for an initially populated 19d states; 19d (bold solid curve), 19 $l>2$ (solid curve), 10*p (dashed curve). (A) shows the experimental results and (B) shows the results of the quantum theory discussed in the text. In particular, note that the d state is rapidly depleted via population of high-l and -p states. At the highest fields shown, a substantial amount of population resides in the high-l states.

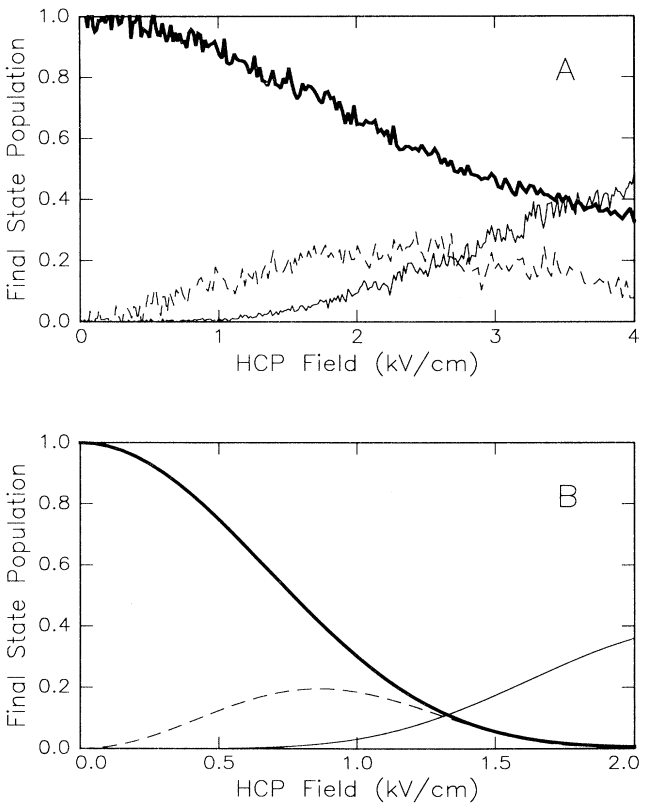

FIG. 7. Analogous to Fig. 6 for an initially populated 19*s state; 19*s (bold solid curve), 19 $l>2$ (solid curve), 19*p (dashed curve). Note that the s state depletes much more slowly than the d states (see Fig. 6) due to its large frequency separation from dipole allowed s-to-p transitions (see Fig. 1). There is only qualitative agreement between experiment and theory, since the field scales differ by a factor of 2.

curve is produced using a voltage ramp with sufficient amplitude to ionize the high-l,m states. The initial-state and p-state curves are obtained using a lower peak ramp voltage and narrow bin widths to reduce the amount of signal from unwanted states. These narrow time bins result in improper relative normalization between the initial-state and p-state curves. Therefore, the p-state curves are normalized so that the maximum p-state signal equals the average of the maximum p-state signal from three different data runs with larger bin widths, which more accurately determine the relative p amplitude. Finally, the field axis on the different scans are normalized so that the field at which the initial state is depleted by 50% and the field at which the p state reaches its maximum value agrees with average field for these quantities from four different data runs.

In Fig. 8(a), the peak fields required to reduce the initial n^*d-state population to its minimum value and the 50% point are shown as a function of n^*. In Fig. 8(b), we plot the HCP field at which the probability for transferring population from an n^*d level to the n^*p state is maximized vs n^*. Analogous plots are shown for redistribution from n^*s in Figs. 8(c) and 8(d), with the exception that the s-state population does not exhibit any clear local minimum. The field values are obtained from four separate data runs and the errors are typically 15–20 %.

Figures 6(b), 7(b), and 8(a)–8(d) also show the results of a quantum-mechanical calculation of the redistribution process. The theoretical curves are the result of a numerical integration of the time-dependent Schrödinger equation, using a finite spherical basis set and the dipole approximation. The calculation assumes a Gaussian HCP of 500-fs duration. The radial matrix elements are calculated using a standard Numerov integration algorithm [8] and the quantum defects of the Na Rydberg states [9]. For the field strengths shown, up to 200 states are necessary to describe the redistribution from an initial n^*s or n^*d state. The results of these calculations are in agreement with those of Reinhold, Shao, and Burgdorfer [5].

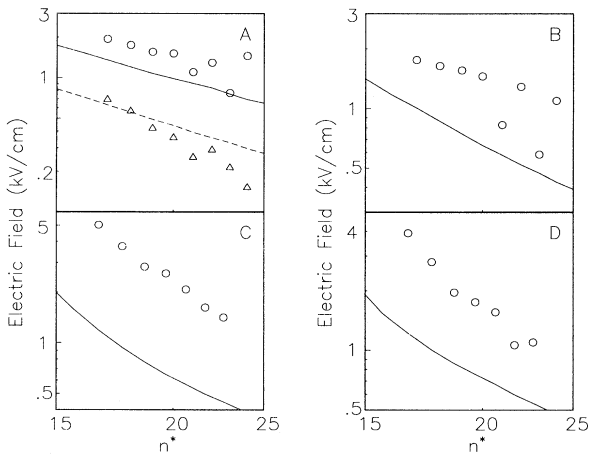

FIG. 8. Experimental (discrete points) and theoretical (continuous curves) field values required for population transfer for initially populated s and d states as a function of n^*. (A) Field required to reduce the initial d-state population to 50% (triangle, experiment; dashed curve, theory) and to minimize the d state population (circle, experiment; solid curve, theory). (B) Field required to maximize the population in the n^*p state from an initial n^*d level (circle, experiment; solid curve, theory). (C) Field required to reduce the initial s state to 50% (circle, experiment; solid curve, theory). (D) Field required to maximize the n^*p-state population from the initial n^*s state (circle, experiment; solid curve, theory). The experimental error bars are approximately 20%. Note that there is agreement between experiment and theory on the n^* dependence of the fields.

The results of the simulation for representative s and d initial states are shown in Figs. 6(b) and 7(b), respectively. There is some agreement with the experimental data. In Fig. 7 the agreement is only qualitative since the field scales for the experimental and theoretical curves differ by a factor of 2. The largest discrepancy between experiment and theory can be seen in the s-state curves. The s-state data consistently show significantly less depletion than predicted at any given field value. The difference can be attributed (at least in part) to our inability to completely resolve the s-state signal from that of the higher-l states.

The differences between the calculated and measured fields are shown explicitly in Figs. 8(a)–8(d). It is important to note that in some curves the data consistently falls above the theoretical prediction, while in others it falls below the expected values. This observation suggests that the discrepancy between the measured and calculated redistribution probability is due to differences in the spectral intensity distribution between the true HCP and the Gaussian model pulse, not to an overall field calibration. In particular, s-state depletion relies on transitions to p states at relatively high ($\approx 10\ \mathrm{cm}^{-1}$) frequencies, and the experimental 50% depletion requires a factor of 3 higher peak than predicted by theory. On the other hand, d-state depletion can proceed primarily through low-frequency ($<1\ \mathrm{cm}^{-1}$) transitions to f states, and experimentally, 50% depletion requires fields that are comparable to or lower than those predicted. Therefore, these results suggest that the power spectrum of the true HCP is more sharply peaked at lower frequencies than that due to a 500-fs Gaussian at these field strengths. Although previous studies have observed negligible variation in the HCP duration with decreasing wafer bias voltage [3,10], it is possible that the bandwidth of the pulse has a non-negligible bias voltage dependence at these low voltages, which could be partially responsible for the discrepancy.

The theoretical curves in the log plots in Figs. 8 are nearly linear, suggesting fields that scale as powers of n^*. All of the curves have slopes ranging from approximately -2 to -4. This is the expected result from perturbation theory. First, consider single-photon transitions. In this case, the probability for transferring population from one state to another is simply $P=\Gamma\sigma F^2$, where Γ depends on the transition frequency and pulse bandwidth, σ is the transition cross section, and F is the HCP field amplitude. σ scales as n^{*4} for $l \ll n^*$ and as n^{*3} for $l \approx n^*$ for transitions between states n^*l and $n^*l \pm 1$. Also, if the change in transition frequency with increasing n^* is small compared to the pulse bandwidth, then Γ is nearly in-

dependent of n^*. Therefore, for a fixed transfer probability, the requisite fields vary as n^{*-2} for transitions between low-l states and as $n^{*-3/2}$ for transitions involving high-l states [11]. Inverse powers greater than 2 can be caused by at least two different sources. The first is the n^* dependence of Γ. Variations in Γ with increasing n^* become significant if the transition frequencies fall outside of the HCP bandwidth. Since the pulse spectrum has both low- and high-frequency limits (there can be no dc component in the field), Γ decreases rapidly if the transition frequencies (i.e., the values of n^*) get too large or too small. The second source is multiphoton transitions. If we consider transitions between states with $l \ll n^*$ and if the intermediate transitions in the multiphoton process all occur between states with the same value of n^*, then each radial matrix element scales as n^{*2}, and each energy detuning scales as n^{*-3} [11]. Therefore, the transition probability can be written as $P=\Gamma' n^{*2(5k-3)}F^{2k}$, for a k photon process. The field required to transfer a given population fraction scales as $n^{*-(5k-3)/k}$. So for $k=1$ and $k \gg 1$, F will be proportional to n^{*-2} and n^{*-5}, respectively. If the transitions are between states with $l \approx n^*$, then the same arguments above apply except for the different scaling of the radial matrix elements. So for transitions between high-l states, F is proportional to $n^{*-3/2}$ and $n^{*-9/2}$ for $k=1$ and $k \gg 1$, respectively.

The d-state redistribution data in Figs. 8(a) and 8(b) are in reasonable agreement with those predicted by theory. The slopes of the s-state redistribution data in Figs. 8(c) and 8(d) are also in fairly good agreement with theory. The major source of error in the experimental data is the imperfect resolution of the different final-state peaks in the time-of-flight spectrum. The data shown in Fig. 8 are averages over several data runs using different temporal widths for the time bins used to integrate the signal in each final-state peak. As mentioned previously, we estimate the typical errors in the field values reported in Fig. 8 to be 15–20 %.

The data and calculation both show a gradual decrease in the maximum population transferred from d states to p states with increasing n^*. Conversely, the transfer of population from s to p increases with increasing n^*. Both of these features can be attributed to increased s-to-p coupling as the transition frequency moves toward the peak of the HCP bandwidth. For n^* values in the low twenties, 25% of s- or d-state population can be transferred to the nearest p state. However, for $n^* \approx 16$, the p state typically reaches a maximum population of less than 10% for an initial s state and over 40% for an initial d state.

IV. REDISTRIBUTION USING TWO TIME DELAYED HCPs

The results of the single-pulse experiments show that the population transfer process can be adequately described using quantum mechanics and a model HCP. Theoretically, the redistributed population is coherent, and there is a well-defined phase difference between any two states at any time during or after the HCP. After the HCP, the wave function of the Rydberg electron can be written as a superposition of different stationary energy and angular-momentum states. The amplitude of each eigenstate in the superposition contains the familiar time-dependent phase factor e^{-iEt}, where E is the energy of the eigenstate in atomic units. Therefore, the spatial distribution of the final superposition state is nonstationary.

The dynamic evolution of this nonstationary state is extremely complex, and in general, it will be quite different from that of radial or angular Rydberg wave packets [12] or anti wave packets [6,13] that have been produced using short laser pulses. The difference in the dynamics of the states are linked to the differences in the excitation mechanisms. Short laser pulses only change that part of the Rydberg wave function that is near the nucleus. Probability amplitude can be added to the small radius part of the Rydberg potential via excitation from a lower-lying state, or it can be removed from the core region via deexcitation or ionization. In addition, the changes to the Rydberg wave function are symmetric with respect to the positive and negative directions along the laser polarization. On the other hand, HCPs can alter the Rydberg wave function near the nucleus as well as far from it. Furthermore, the unipolarity of the HCP automatically introduces an asymmetry in the Rydberg wave function, as long as the pulse duration is shorter than the Kepler period of the Rydberg orbit. Hence, a true HCP can be extremely useful for creating new types of dynamic states in atoms.

Of course, the description in the last paragraph hinges on the assumption of a coherent redistribution process. This assumption must be verified experimentally. Therefore, we have performed an experiment that examines the redistribution of Rydberg population using two temporally separated HCPs. The level of coherence in the population transferred to each state is determined by looking for a change in the transfer probability as a function of the time delay between the two pulses.

The observed changes in the redistribution process as a function of delay between two pulses can be described in several different ways. For simplicity, consider a nondegenerate two-level system which is subjected to two temporally separated, phase-coherent electromagnetic pulses. The following descriptions can be generalized to include an arbitrary number of interacting states. The pulses need not be identical. Assume that before the pulses arrive, all population is in level $|1\rangle$. The first pulse transfers some population to state $|2\rangle$. The amplitudes of states $|1\rangle$ and $|2\rangle$ include time-dependent phase factors $\exp(-iE_1t)$ and $\exp(-iE_2t)$, respectively. Therefore, they acquire the phase at different rates due to their different energies. The second pulse will transfer population from $|1\rangle$ to $|2\rangle$ and from $|2\rangle$ to $|1\rangle$. The probability amplitude in each state after the second pulse depends on the relative phase between the two states during the second pulse. This phase difference is proportional to the time delay between the two pulses. In fact, the population left in either state will exhibit a sinusoidal modulation as a function of the delay. Hence, the transfer probability is analogous to the intensity at the output of an

optical interferometer as a function of the difference in optical path length between the two legs of the interferometer. The two pulses act as beam splitters that split and the recombine probability amplitudes [6,14].

Alternatively, we can consider the two pulses to be components of a single field. The frequency spectrum of the field will depend on the bandwidth of the two separated pulses as well as the separation between them. The presence of the two pulses produces a modulation in the frequency spectrum of the total field. As the delay between the two pulses is increased, the oscillations move through the frequency spectrum, producing delay-dependent maxima and minima in the field intensity at the $|1\rangle$ to $|2\rangle$ resonance frequency.

A third, equivalent description can be formulated if we consider the time-dependent distribution of charge on the atom. Before the first pulse, the charge distribution is stationary. After the pulse, the atom is left in a linear superposition of $|1\rangle$ and $|2\rangle$. The spatial charge distribution of this superposition state will oscillate with a frequency (E_2-E_1) a.u. During the second pulse, the interaction of the field with oscillating charge distribution will depend on the relative phase between the field and the oscillation of the superposition state.

All three of the above descriptions rely critically on phase coherence between the two pulses and between the atom and the pulses. In recent laser experiments, two phase-coherent time-delayed pulses have been produced by splitting a laser pulse using a Michelson interferometer [6]. However, phase coherence is never a problem with a true HCP, and two time-delayed pulses will always be coherent, even if the pulses originate from two separate sources. The "phase" of the HCP is fixed by the sign of the bias voltage on the GaAs wafer. In our experiments, the two HCPs are created using two different GaAs wafers that are illuminated by two time-delayed laser pulses (see Fig. 9). Note that since the laser pulses convey no optical phase information to the HCPs, the jitter in the delay between the two pulses need only be small compared to the 0.5-ps duration of the HCP. Therefore, the stability constraints are greatly relaxed over laser experiments that require relative pulse jitter much less than the femtosecond optical period [6].

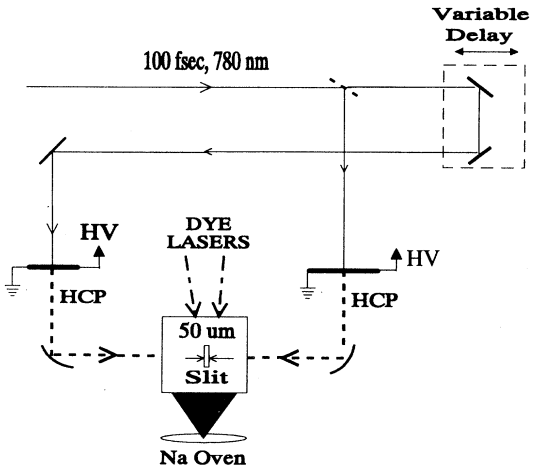

FIG. 9. Schematic of the two-pulse apparatus showing the symmetric orientation of the HCP generators and the 50-μm collection slit used to achieve adequate temporal resolution. Note that no transient attenuators are used for the two-pulse experiments.

The two HCPs enter the interaction region antiparallel to each other and at right angles to the dye laser and atomic beams, as shown in Fig. 9. This geometry gives a temporal resolution for the relative pulse decay, which is limited to the pulse transit time beneath the extraction hole. Therefore, for the two-pulse experiments, electrons are extracted through a 50-μm slit in the upper field plate. This gives us a temporal resolution of <200 fs, which is less than half of the HCP duration.

Figures 10(a) and 10(c) show the population in the 17^*d and 17^*p levels as a function of delay between two pulses, each with a peak field of 700 V/cm. The initial state for the scan is 17^*d. The population in both states shows strong periodic variations over nanosecond time scales [Figs. 10(a) and 10(c) show only portions of the complete scan]. Hence, at these peak fields, the coherence of the redistribution process is clearly maintained. The 17^*d population in Fig. 10(a) shows modulations at two different frequencies. A discrete Fourier transform of the data displayed in Fig. 10(a) is shown in Fig. 10(b). Two peaks corresponding to the single-photon transitions between 17^*d to 17^*f and 17^*d to 17^*p can clearly be seen. These are the two dominant transitions expected from lowest-order perturbation theory. In addition, the area under the d-to-f resonance is slightly larger than that under the d-to-p peak, in agreement with the transition rate arguments presented previously.

The p-state population displayed in Fig. 10(c) shows a strong rapid oscillation and a weaker broad modulation. The Fourier transform of this scan, which is shown in Fig. 10(d), confirms that the p state is modulated at the same transition frequencies as the d state. However, the amplitude and phase of the modulation are different. The implicit assumption of insignificant initial-state depopulation in lowest-order perturbation theory predicts that the p-state population should oscillate at the d-to-p transition frequency only. Therefore, the appearance of the small d-to-f transition peak in Fig. 10(d) shows that lowest-order perturbation theory has already broken down for these states at fields of 700 V/cm. Ionization of the $17d$ state is negligible until the peak HCP field is an order of magnitude or more larger.

Figures 11(a)–11(d) show a numerical simulation of the data displayed in Figs. 10(a)–10(d) for a peak HCP field of 400 V/cm. The calculation involves the same numerical integration of the time-dependent Schrödinger equation described above, assuming a Gaussian HCP shape. All angular-momentum states corresponding to at least five different principal quantum numbers centered on the initial state are used in the calculation. All of the experimental and theoretical results presented here were obtained with the two pulses polarized in opposite directions.

As is the case with single-pulse redistribution, the theoretical results are in qualitative agreement with the

data. However, the field strength necessary to reproduce the observed structure can be up to a factor of 2 lower than observed experimentally. Nevertheless, the qualitative agreement suggests that we can adequately describe the experimental conditions. The reduced resolution of the Fourier transform spectra in Fig. 11 compared to that in Fig. 10 is due to the limited maximum delay in the calculation. The calculation used a 200-ps delay scan while the data in Fig. 10 is a scan over an 800-ps delay. Note that the "zero" delay point in Figs. 10(a) and 10(c) was picked arbitrarily and does not correspond to the time where the two HCPs overlap. The lack of an absolute scale is unimportant here due to the periodicity of the signal.

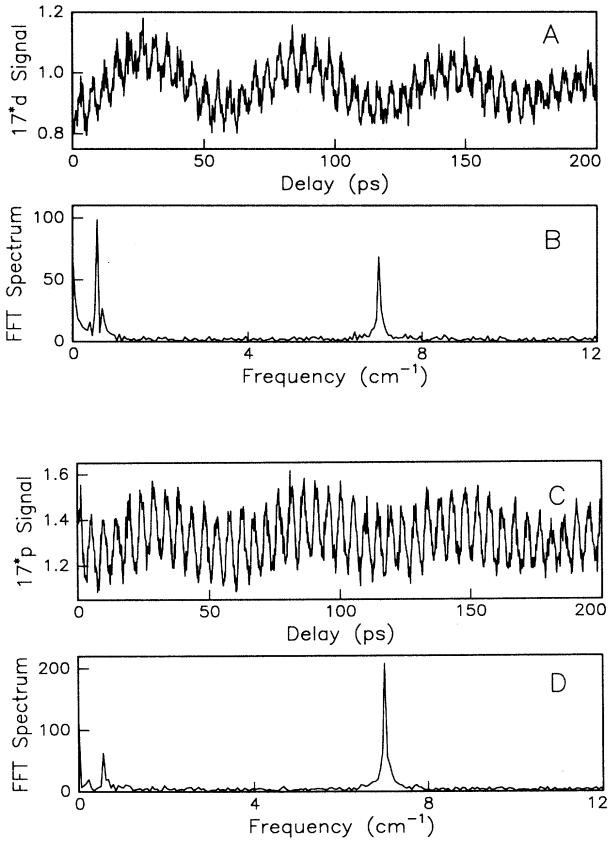

FIG. 10. (A) and (C) display the amount of signal in the $17d$ and 17^*p states, respectively, as a function of the relative delay between two HCPs, with a peak amplitude of 700 V/cm. The initial Rydberg state is $17d$ and the two HCPs have opposite polarity. Both (A) and (C) show strong periodic modulations at slow and fast frequencies. The zero on the delay axis is the same for both (A) and (C), but does not correspond to zero delay between the two pulses. (B) and (D) show the results of a discrete Fourier transform of the data in (A) and (C). The Fourier transform spectra are obtained from an 800-ps scan, only part of which is shown in (A) and (C). Note that two distinct peaks corresponding to transitions from $17d$ to $17f$ and $17d$ to 17^*p appear in the transform spectra. The appearance of the d-to-f transition in the p-state signal is caused by depletion of the d state and signifies that lowest-order perturbation theory is not strictly valid, even at this low-field strength.

Aside from verifying the coherence of the redistribution process, the interferometric method is a useful and powerful spectroscopic tool. First, low-intensity scans, like those shown in Fig. 10, can be used to determine energy-level splittings with moderately high resolution. Note that the peak widths in Figs. 10(a) and 10(c) are on the order of 2 GHz (only a portion of the total 800-ps scan is shown). The frequency resolution is limited only by the maximum delay time between the two pulses. Although the energy levels for most of the lower-angular-momentum Rydberg states in Na are already known to good precision, the technique might be useful for characterizing less well known systems at GHz and THz frequencies. Second, by observing the transitions that dominate the interferograms as a function of field, we can study the evolution from perturbative to nonperturbative dynamics in the population transfer process.

Discrete Fourier transforms of experimental and theoretical interferograms for population transfer to the 20^*p state from an initially populated 20^*s level are shown in Figs. 12(a) and 12(b), respectively. The peak

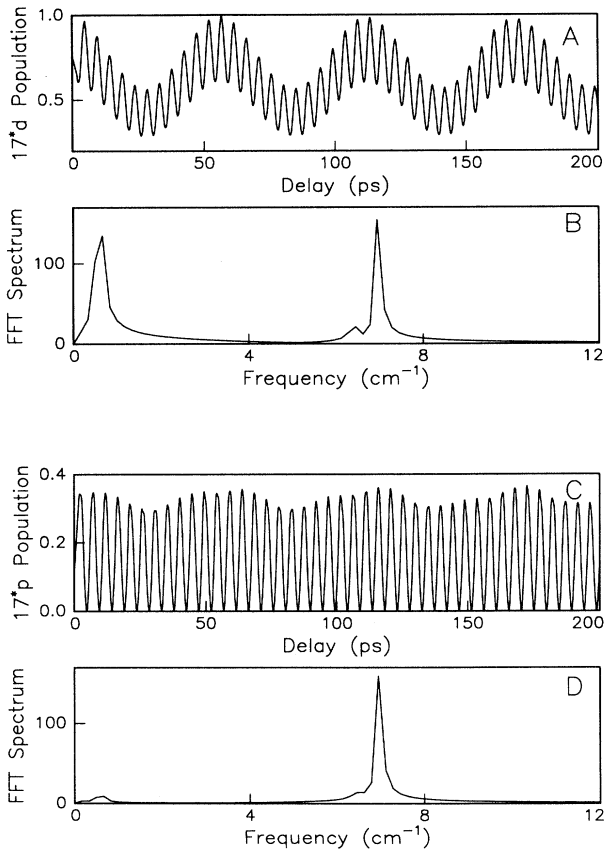

FIG. 11. Theoretical reproduction of the experimental results shown in Fig. 10 as discussed in the text. The relative phase shifts between theory and experiment are due to the arbitrary zero point in the experimental scan. Note that the agreement between theory and experiment is only qualitative, since the theoretical field strength used is only 400 V/cm. The relatively poor frequency resolution in the transform spectra in (B) and (D) is due to the limited maximum delay of 200 ps.

field used in the experiment is 430 V/cm while 220 V/cm was used in the calculation to achieve better qualitative agreement with the data. The predominant transition frequencies appear as peaks in the spectrum. The effect of direct s-to-d transitions and p-to-d transitions in the p-state population is apparent. However, the Fourier spectra show that the 20^*s to 20^*p transition dominates, as predicted by perturbation theory.

Analogous spectra are shown in Figs. 13(a) and 13(b) at substantially higher peak fields of 1.8 kV/cm (experiment) and 800 V/cm (theory). Strong transitions involving the absorption of one, two, and three photons are visible. Note that the amplitude of the peaks corresponding to higher-order transitions are comparable in height to the single-photon features. Hence, perturbation theory is no longer valid in this regime. The HCP field required to produce a few percent of ionization from the same initial state is >6 kV/cm. Therefore, perturbative analysis becomes invalid for field strengths much lower than those necessary for ionization.

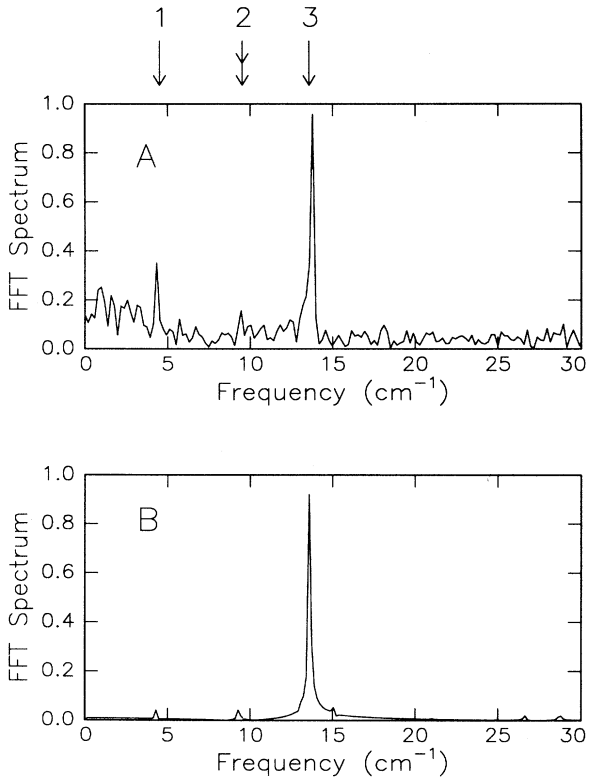

FIG. 12. Fourier transform of (A) experimental and (B) theoretical interferograms for the transfer of population to the 20^*p level by two oppositely polarized HCPs from an initially populated 20^*s state. One large and two smaller peaks can be observed in both transform spectra. The arrows correspond to transitions from (1) 20^*p to $20d$, (2) 20^*s to $20d$, and (3) 20^*s to 20^*p. The experimental HCP field is 430 V/cm, while the theoretical field is 220 V/cm. Note in particular the appearance of peak (2), which is the result of a two-photon transition that does not directly involve the p state that is detected.

V. DISCUSSION

In general, the qualitative agreement between theory and experiment for both the single- and double-pulse redistributions rapidly disappears with increasing field strength. Typically, the agreement holds for fields comparable to those needed to maximize the transfer of population to the nearest p state. One possible explanation for the lack of agreement in high fields is the decrease in selectivity of our field ionization technique when a large number of states are populated. Instead of detecting the population in a single state, we actually measure the population in one state plus part of the population in several

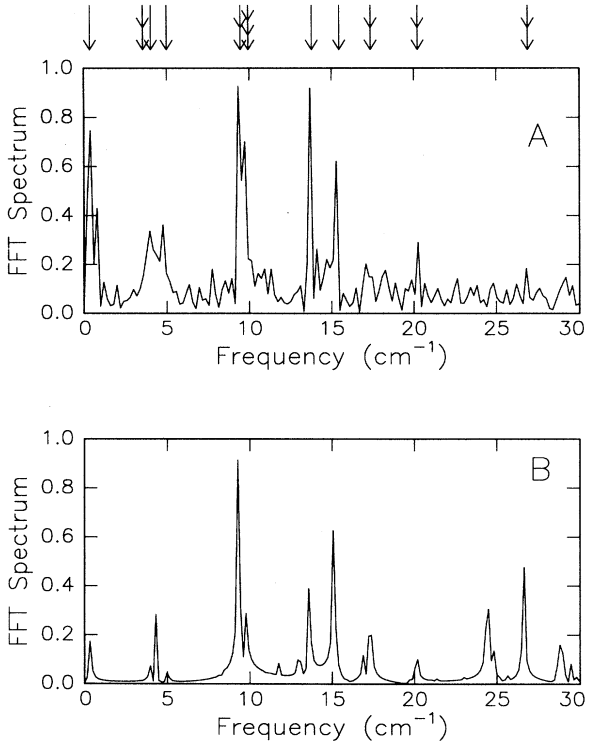

FIG. 13. (A) and (B) are analogous to Fig. 12 at peak fields of 1.8 kV/cm and 800 V/cm, respectively. Note the large number of peaks in both the experimental and theoretical spectra. Peaks corresponding to transitions involving the absorption of at least one, two, and three photons are visible in both (A) and (B). The number of heads on each arrow corresponds to the minimum number of photons that must be absorbed for a given transition. More peaks are visible in the theoretical spectra than in the experimental one, including several higher-frequency peaks at >30 cm^{-1}. From left to right, (1) the single arrows label transitions $20d$-$20f$, 20^*p-$20d$, 19^*p-$19d$, 20^*s-20^*p, and 20^*s-19^*p; (2) the double arrows label transitions 20^*p-$20f$, 20^*s-$20d$, $20d$-21^*s, 20^*s-$19d$, and 20^*s-21^*s; and (3) the triple arrow labels the 20^*s-$20f$ transition. The large peak amplitude ratio of the one-photon to two-photon transitions in Figs. 12 is not seen in these figures. In fact, two and three-photon transitions that do not directly involve the p state are more important to the p-state redistribution than direct single-photon processes from the s state. This is direct evidence that perturbation theory does not adequately describe the redistribution for these states at these field strengths.

other states. Unfortunately, we have no good quantitative method for measuring how much of the signal we detect comes from different unwanted states. Therefore, a comparison with theory becomes difficult. Another source of error is population transfer due to noise in the HCP. Once the peak field strength is high enough to saturate transitions, the relative importance of low-level noise and the small nonunipolar components in the HCP increases. Furthermore, the two-pulse experiments are sensitive to relative amplitude jitter, especially in strong fields where transitions are driven past saturation with a single pulse. This relative amplitude noise is not a problem in configurations where a single pulse is split into two using a Michelson interferometer. In that case there is amplitude noise, but not relative jitter. Undoubtedly, both the decrease in final-state selectivity, pulse noise, and deviations in the temporal pulse shape from the Gaussian model are major contributors to the discrepancy between theory and experiment at high field.

Our ability to theoretically predict (at least qualitatively) the results of the coherent population transfer process, as well as ionization with HCPs, indicates that the basic interaction between Rydberg atoms and these pulses is reasonably well understood. Therefore, these pulses may now be used as tools for probing and creating dynamic states in atoms. Due to the unique unipolar nature of HCPs, they may be used to excite and probe time-dependent asymmetries in atomic charge distributions as well as asymmetries in momentum distributions. The ability of these pulses to detect orientation dependences in Rydberg states has already been established [2]. Future experiments may be aimed at using these pulses to excite transient dipole moments in atomic systems to change the angular distribution of photoelectrons or to modulate collision cross sections.

In summary, we have studied the coherent redistribution of population among Rydberg states in Na. The redistribution process is very efficient, transferring essentially all of the initial-state population to other bound states. In particular, high-angular-momentum states are easily populated from low-angular-momentum states in a single HCP. The redistribution process has been studied as a function of peak field for a single HCP and as a function of the relative time delay between two HCPs. The latter technique allows us to observe the evolution from perturbative to nonperturbative dynamics. Generally, the results are in qualitative agreement with numerical quantum-mechanical calculations.

ACKNOWLEDGMENTS

We thank T. J. Bensky for technical assistance. This work was supported by the Office of Naval Research.

[1] R. R. Jones, D. You, and P. H. Bucksbaum, Phys. Rev. Lett. **70**, 1236 (1993).

[2] R. R. Jones, N. E. Tielking, D. You, C. S. Raman, and P. H. Bucksbaum, Phys. Rev. A **51**, R2687 (1995).

[3] D. You, R. R. Jones, D. R. Dykaar, and P. H. Bucksbaum, Opt. Lett. **18**, 290 (1993).

[4] C. O. Reinhold, M. Melles, H. Shao, and J. Brugdorfer, J. Phys. B **26**, L1 (1993); K. J. LaGattuta and P. Lerner, Phys. Rev. A **49**, R1547 (1994); A. Bugacov, B. Piraux, M. Pont, and R. Shakeshaft, *ibid.* **51**, 1490 (1995); C. D. Schwieters and J. B. Delos, *ibid.* **51**, 1023 (1995); **51**, 1030 (1995).

[5] C. O. Reinhold, H. Shao, and J. Burgdorfer, J. Phys. B **27**, L469 (1994).

[6] R. R. Jones, C. S. Raman, D. W. Schumacher, and P. H. Bucksbaum, Phys. Rev. Lett. **71**, 2575 (1993).

[7] N. E. Tielking, T. J. Bensky, and R. R. Jones, Phys. Rev. A **51**, 3370 (1995).

[8] M. L. Zimmerman, M. G. Littman, M. M. Kash, and D. Kleppner, Phys. Rev. A **20**, 2251 (1979).

[9] W. C. Martin and R. Zalubas, J. Phys. Chem. Ref. Data **10**, 155 (1981).

[10] P. K. Benicewicz, J. P. Roberts, and A. J. Taylor, J. Opt. Soc. Am. B **11**, 2533 (1994).

[11] H. A. Bethe and E. E. Salpeter, *Quantum Mechanics of One- and Two-Electron Atoms* (Springer-Verlag, Berlin, 1957).

[12] A. ten Wolde, L. D. Noordam, H. G. Muller, A. Lagendijk, and H. B. van Linden van den Heuvell, Phys. Rev. Lett. **61**, 2099 (1988); J. A. Yeazell, M. Mallalieu, J. Parker, and C. R. Stroud, Jr., Phys. Rev. A **40**, 5040 (1989); J. A. Yeazell and C. R. Stroud, Jr., *ibid.* **43**, 5153 (1991).

[13] L. D. Noordam, H. Stapelfeldt, D. I. Duncan, and T. F. Gallagher, Phys. Rev. Lett. **68**, 1496 (1992).

[14] L. D. Noordam, D. I. Duncan, and T. F. Gallagher, Phys. Rev. A **45**, 4734 (1992).